Available online at www.sciencedirect.com

SciVerse ScienceDirect

Procedia Computer Science 9 (2012) 689 – 698

Procedia Computer Science

International Conference on Computational Science, ICCS 2012

An efficient two-grid method for a two-phase mixed-domain model of polymer exchange membrane fuel cell

Mingyan He[a], Ziping Huang[a,b], Cheng Wang[a,*], Pengtao Sun[c]

[a]*Department of Mathematics, Tongji University, Shanghai, 200092, P.R. China*
[b]*Chinese-German College, Tongji University, Shanghai, 200092, P.R. China*
[c]*Department of Mathematical Sciences, University of Nevada Las Vegas, 4505 Maryland Parkway, Las Vegas, NV 89154, USA*

Abstract

In this paper, an efficient and fast numerical method is studied and implemented for a simplified two-phase mixed-domain model of polymer exchange membrane fuel cell (PEMFC), which fully incorporates both the anode and cathode sides, including the conservation equations of mass, momentum, water vapor concentration, liquid water saturation and water content. The proposed numerical algorithm is based on the two-grid discretization technique, the combined finite element-upwind finite volume method and some other appropriate linearization schemes. The original nonlinear partial differential equations are only solved on the coarse grid while the fine grid approximation solution is obtained linearly. Therefore the computational time can be reduced tremendously compared with the traditional one-grid method. Numerical experiments of the two-grid method and conventional method for a two-phase mixed-domain fuel cell model are carried out, showing that the presented method is effective and accurate for the numerical simulation of PEMFC.

Keywords: PEMFC, two-phase model, two-grid method, finite element-upwind finite volume method

1. Introduction

Numerical modeling and simulation have been an important tool for the design and optimization of polymer exchange membrane fuel cell (PEMFC). Water management is a key issue in PEMFCs, and is a significant technical challenge. Sufficient water are needed in the membrane to maintain high proton conductivity, however, excess liquid water in the electrode can cause water flooding, and hinder the transport of the reactant from the gas channels to the catalyst layers. To optimize water management, many approaches are used to simulate the multi-phase phenomenon occurring in fuel cell, for which the multi-phase mixture (M^2) model [1, 2, 3, 4, 5] and multi-fluid model [6, 7, 8, 9, 10] are mainly developed. Recently, a mixed-domain model, which maintains a consistent treatment of water transport in the membrane electrode assembly (MEA), has been developed in [11] based on the traditional two-fluid model.

A fundamental fuel cell model consists of five principles of conservation: mass, momentum, species, charge, and thermal energy. These complex nonlinear partial differential equations (PDEs) are formed by coupled nonlinear

*Corresponding author
Email addresses: hemingyan1985@yahoo.com.cn (Mingyan He), huangziping@tongji.edu.cn (Ziping Huang), wangcheng@tongji.edu.cn (Cheng Wang), pengtao.sun@unlv.edu (Pengtao Sun)

doi:10.1016/j.procs.2012.04.074

relationship among the common Navier-Stokes equations and convection-diffusion-reaction equations. There is no doubt that it is a huge challenge to solve this complex system of nonlinear PDEs in an efficient and robust manner. Comparing to the relatively plentiful literature on modeling and experimental study of fuel cells, there are less study contributing to the numerical method of two-phase transport PEMFC model. P. Sun et al [12, 13, 14, 15, 16] lead the field in numerical studies for PEMFC due to their cutting edge work on the efficient numerical methods for the M^2 model of PEMFC. In [13], the streamline-diffusion and Galerkin-least-squares finite element methods are applied to a 2D steady-state two-phase model in the cathode of PEMFC to get accurate physical solutions with fast convergence. Using Kirchhoff transformation in [14], the numerical instability due to the discontinuous and degenerate water diffusivity arising from M^2 model is overcome by a well developed Dirichlet-Neumann alternating iterative domain decomposition method. The combined finite element-upwind finite volume method [13, 17, 16] is also used in the numerical simulation to stabilize the dominant convection term in gas channels. However, the effective numerical method for the multi-fluid model of PEMFC is still far from satisfactory. The conventional method, such as finite volume method, is commonly used in the numerical simulation for the multi-fluid model [10, 11] based on the commercial computational fluid dynamic (CFD) software.

Two-grid method was originally developed by J. Xu in the literature [18, 19] to solve the nonsymmetric and nonlinear elliptic boundary value problems. The algorithm gives the approximate solution of the original problem on a coarse mesh first, then the symmetric and linear part of the equation are modified on a fine mesh. Theoretical analysis also shows that the approximate solutions of the two-grid method have the same convergence rate with that of one-grid method by directly solving differential equations on the fine grid. Meanwhile, the computational cost is greatly reduced [20, 21, 22]. The two-grid method has been successfully used for solving linear elliptic boundary value problems, Stokes equation [23], the steady-state Navier-Stokes equations [24] and other partial differential equations.

Our goal in this paper is to explore and develop a two-grid algorithm for efficiently solving the coupled nonlinear PDEs of the two-phase mixed-domain PEMFC model proposed by H. Meng in [11]. The rest of this paper is organized as follows. Governing equations for a simplified two-phase mixed-domain model of PEMFC are introduced in Section 2. In Section 3, combining finite element method, upwind finite volume method and two-grid method, a new numerical algorithm is designed to solve the proposed model. Numerical experiments of several practical cases are presented in Section 4, showing that our developed numerical schemes significantly improve the computational performance in the senses of efficiency and lossless accuracy.

2. A two-phase mixed-domain model of PEMFC

Without considering the current collectors, a fuel cell is typically divided into seven subregions: the anode gas channel (GC), anode gas diffusion layer (GDL), anode catalyst layer (CL), ionomeric membrane, cathode GC, cathode GDL and cathode CL. On the basis of the traditional two-fluid model, a 2D non-isothermal, mixed-domain, two-phase model of PEMFC was first studied in [11]. In this paper we restrict our model to isothermal case, investigate the interactions among the principle physical solutions arising from the existing models, and reformulate the water species equations to become a suitable strong PDE form for the purpose of finite element discretization.

2.1. Governing equations

Water management is critical to achieve high performance for PEMFC. As it is referred to as balancing membrane hydration with flooding avoidance, there are two conflicting needs: to hydrate the polymer electrolyte and to avoid flooding in porous electrodes and GDL for reactant/product transport [2]. Therefore, in order to focus on water management topics, without loss of generality, we typically consider water as the only component in the following simplified species concentration equation.

First, the conservation equations of mass, momentum and water species concentrations in the gaseous phase are established as [2, 11].

Mass and momentum conservation. The generic mass and momentum conservation equations, valid for all fuel cell components except current collectors and membrane, can be written for water vapor flow as

$$\nabla \cdot (\rho_g \vec{u}_g) = 0, \tag{1}$$

$$\frac{\rho_g}{\varepsilon^2(1-s)^2}\nabla \cdot (\vec{u}_g \vec{u}_g) = -\nabla p_g + \mu_g \triangle \vec{u}_g + S_u, \tag{2}$$

where the additional source term S_u is added in the porous materials based on the Darcy's law considering the liquid water effect

$$S_u = -\frac{\mu_g}{K_{rg}K}\vec{u}_g, \tag{3}$$

where K_{rg} is the relative permeability for gaseous phase and K the absolute permeability, defined in Table 1 and 2.

Water vapor species conservation. Water concentration equation in gaseous phase is defined as follows with respect to concentration C_w,

$$\nabla\cdot(\vec{u}_g C_w) = \nabla\cdot(D_w^{eff}\nabla C_w) + S_w, \tag{4}$$

considering the liquid water effect, D_w^{eff}, the effective gaseous species diffusion coefficients, namely the constant diffusivity in gaseous water region, is further defined as $D_w^{eff} = D_w(1-s)^{1.5}$. In the catalyst layers, the water phase is assumed to be in thermodynamic phase equilibrium with water vapor, and its transport process is considered based on the "fictitious water concentration" treatment [25, 26] using the following water diffusivity [11]

$$D_w = \begin{cases} \varepsilon_{cl}^{1.5} D_{gas} + \varepsilon_m^{1.5} D_\lambda \frac{RT}{p^{sat}}\frac{d\lambda}{da} & \text{CLs} \\ \varepsilon^{1.5} D_{gas} & \text{otherwise.} \end{cases} \tag{5}$$

where ε_{cl} and ε_m represent porosity in catalyst layers and membrane, respectively.

Table 1: Physical relationships

Description	Expression
Relative permeability for liquid phase	$K_{rl} = s^3$
Relative permeability for gaseous phase	$K_{rg} = (1-s)^3$
Water content diffusivity	$D_\lambda = \frac{\rho_m}{EW} D_w^m$
Membrane water diffusivity	$D_w^m = \begin{cases} 3.1\times10^{-7}\lambda\left(e^{0.28\lambda}-1\right)e^{-\frac{2346}{T}} & 0<\lambda\le 3 \\ 4.17\times10^{-8}\lambda\left(1+161e^{-\lambda}\right)e^{-\frac{2346}{T}} & \text{otherwise} \end{cases}$
Water saturation pressure	$\log_{10}(p^{sat}) = -2.1794 + 0.02953(T-273.17)$ $-9.1837\times10^{-5}(T-273.17)^2 + 1.4454\times10^{-7}(T-273.17)^3$
Water activity	$a = \frac{C_w RT}{p^{sat}}$
Water content of the membrane	$\lambda = \begin{cases} 0.043 + 17.18a - 39.85a^2 + 36a^3 & 0<a\le 1 \\ 14 + 1.4(a-1) & 1<a\le 3 \end{cases}$
Condensation/evaporation parameter	$h_{pc} = \frac{k_c\varepsilon(1-s)C_w}{2p}\left(1+\frac{\lvert p^v-p^{sat}\rvert}{p^v-p^{sat}}\right) + \frac{k_e\varepsilon s\rho_l}{2W_l}\left(1-\frac{\lvert p^v-p^{sat}\rvert}{p^v-p^{sat}}\right)$
Partial pressure of water vapor	$p^v = C_w RT$
Capillary pressure	$p_c = \left(\frac{\varepsilon}{K}\right)^{0.5}\sigma COS\,\theta_c J(s)$
Leverett's function	$J(s) = \begin{cases} 1.417(1-s) - 2.120(1-s)^2 + 1.263(1-s)s^3 & \theta_c < 90^o \\ 1.417s - 2.120s^2 + 1.263s^3 & \theta_c > 90^o \end{cases}$

In the present two-phase model, water produced in the cathode catalyst layer is assumed to be in vapor phase as in [11, 27]. So the source term S_w is given as follows.

$$S_w = \begin{cases} -\nabla\cdot(\frac{n_d}{F}\vec{i}_e) - \frac{j}{2F} - S_{vl} & \text{in cathode CL} \\ -\nabla\cdot(\frac{n_d}{F}\vec{i}_e) & \text{in anode CL} \\ 0 & \text{otherwise,} \end{cases} \tag{6}$$

where n_d, the electro-osmotic drag coefficient, is a constant value due to the isothermal assumption. $\nabla\cdot\vec{i}_e = -j$, is derived from the continuity equation of proton potential. $\vec{i}_e$ is the current density vector and j the volumetric transfer current of the reaction (or transfer current density), defined by a linear function [13] $j = j_1 - (j_1 - j_2)\frac{x}{l_{cell}}$, which is a linear simplification of Butler-Volmer equation. This is an approximation of transfer current density for a simplified single-phase PEMFC model due to the absence of proton and electron potentials. S_{vl} is the volumetric condensation/evaporation rate, and it represents the interfacial mass-transfer rate of water between the gas and liquid phases, defined as

$$S_{vl} = h_{pc}(p^v - p^{sat}), \tag{7}$$

where the condensation/evaporation parameter h_{pc} and partial pressure of water vapor p^v are determined in Table 1.

In this two-phase model, the liquid water transport is taken into account using the traditional two-fluid method to add the flexibility for studying the finite-rate condensation/evaporation processes [11]. In the following, the conservation equations of liquid water are presented.

Liquid mass conservation. In order to derive the governing equation for the liquid water saturation, the mass conservation equation of liquid water is needed and defined as [11]

$$\nabla \cdot (\rho_l \vec{u}_l) = S_{vl} W_w, \tag{8}$$

where an expression for the condensation/evaporation rate S_{vl} can be found in (7), W_w is water molecular weight.

In the porous medium region, the general momentum of liquid and water vapor conservation equation are reduced to the following expressions of Darcy's law

$$\vec{u}_l = -\frac{K_{rl} K}{\mu_l} \nabla p_l, \tag{9}$$

$$\vec{u}_g = -\frac{K_{rg} K}{\mu_g} \nabla p_g. \tag{10}$$

The so-called capillary pressure p_c, also expressed in Table 1, is defined as the difference of the pressure between the gas and the liquid, leading to

$$p_l = p_g - p_c. \tag{11}$$

Combing the equations (8)-(11), we obtain a conservation equation for the liquid water saturation, given as

$$-\nabla \cdot (\frac{\rho_l K s^3}{\mu_l} \frac{\partial p_c}{\partial s} \nabla s) - \nabla \cdot (\frac{\rho_l \mu_g}{\mu_l} \frac{s^3}{(1-s)^3} \vec{u}_g) = -S_{vl} W_w. \tag{12}$$

Since our numerical studies in this paper only focus on two-phase transport phenomena in porous materials, the liquid water transport in the gas channel is neglected.

Table 2: Physical coefficients and parameters

Parameter	Value	Parameter	Value
Water vapor diffusivity (D_{gas})	$2.6 \times 10^{-5} m^2/s$	Porosity of GDL and CL (ε)	0.6
Porosity of membrane (ε)	0.26	Effective vapor viscosity (μ_g)	$3.1664 \times 10^{-5} kg/m/s$
Vapor density (ρ_g)	$0.882\ kg/m^3$	Liquid water density (ρ_l)	$1000 kg/m^3$
equivalent weight of the membrane (EW)	$1.1\ kg/mol$	Dry membrane density (ρ_m)	$1980\ kg/m^3$
Condensation rate coefficient (k_c)	$5000 s^{-1}$	Evaporation rate coefficient (k_e)	$10^{-4} s^{-1} pa^{-1}$
Liquid water viscosity (μ_l)	$3.5 \times 10^{-4} kg/m/s$	Surface tension (σ)	$6.25 \times 10^{-2} N/m$
Contact angle in GDL (θ_c)	110^o	Contact angle in CL (θ_c)	95^o
hydraulic permeability of GDL and CL (K)	$2 \times 10^{-12} m^2$	Electro-osmotic drag coefficient(n_d)	1.5
Faraday constant(F)	$96485 C/mol$	Operation temperature (T)	$353 K$
Water molecular weight(W_w)	$0.018 kg/mol$	Universal gas constant (R)	$8.31 J/mol/K$
Transfer current density at the left end (j_1)	$20000\ A/m^2$	Transfer current density at the right end (j_2)	$10000\ A/m^2$

Water concentration in membrane. Water content conservation inside the membrane is defined as follows [25]

$$\nabla \cdot (D_\lambda \nabla \lambda) + S_\lambda = 0, \tag{13}$$

where the source term S_λ reads

$$S_\lambda = -\nabla \cdot (\frac{n_d}{F} \vec{i}_e). \tag{14}$$

Governing equations (1), (2), (4), (12) and (13), together with the definitions of physical coefficients and parameters in Table 1 and Table 2, constitute a simplified 2D two-phase mixed-domain transport model of PEMFC. This model can depict the distribution of water along the channel direction.

2.2. Computational domain and boundary conditions

The computational domain and its geometric sizes are schematically shown in Fig. 1, where the horizontal x-axis represents the flow direction and the vertical y-axis points to the through-plane direction.

Equations (1), (2), (4), (12) and (13) form a simplified two-phase model of PEMFC with six unknowns: $\vec{u}_g$ (two components), p_g, C_w, s and λ. Table 3 indicates the simulation subdomains held for each principle unknown. Only in the subdomains checked by "√" shall the corresponding unknown be necessarily computed, otherwise, the unknown is meaningless and specified as Dirichlet boundary condition in those subdomains.

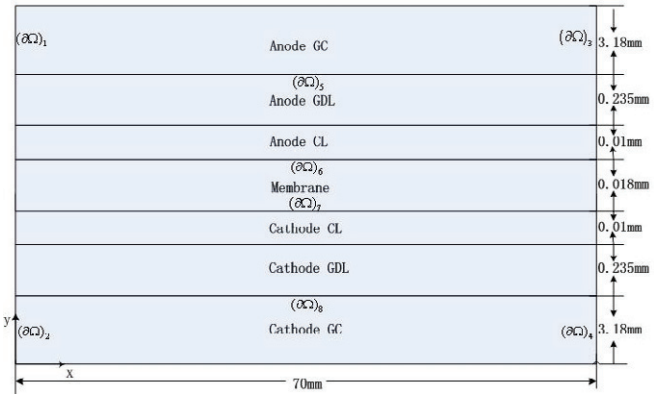

Figure 1: Computational domain

Table 3: The occupancy status of principle unknowns in PEMFC

Unknowns	Anode GC	Anode GDL	Anode CL	Membrane	Cathode CL	Cathode GDL	Cathode GC
$(\vec{u}_g, p_g)$	√	√	√	×	√	√	√
C_w	√	√	√	×	√	√	√
s	×	√	√	×	√	√	×
λ	×	×	×	√	×	×	×

For flow field equation (1) and (2), the following boundary conditions are held in terms of $\vec{u}_g = (u_1, u_2)$ and p_g:

$$\begin{array}{ll} u_1 = u_1|_{inlet},\ u_2 = 0 & \text{on } (\partial\Omega)_1, (\partial\Omega)_2, \\ (p_g I - \mu_g \nabla \vec{u}_g) \cdot \vec{n} = 0 & \text{on } (\partial\Omega)_3, (\partial\Omega)_4, \\ u_1 = 0,\ \ u_2 = 0 & \text{otherwise}, \end{array} \tag{15}$$

where $u_1|_{inlet}$, specified as a parabolic-like function, is given in (25).

For water vapor concentration equation (4), the following boundary conditions are held to ensure equal water flux at the interfaces and specify entry water vapor concentration at the inlet:

$$\begin{array}{ll} C_w = C_{in} & \text{on } (\partial\Omega)_1, (\partial\Omega)_2, \\ (D_w^{eff} \frac{\partial C_w}{\partial n})|_{cl} = (D_\lambda \frac{\partial \lambda}{\partial n})|_m & \text{on } (\partial\Omega)_6, (\partial\Omega)_7, \\ \frac{\partial C_w}{\partial n} = 0 & \text{otherwise}. \end{array} \tag{16}$$

For liquid water saturation equation (12), Dirichlet boundary condition is proposed on the interface of GDL and channel shown as follows:

$$\begin{array}{ll} s = s_{CH,GDL} & \text{on } (\partial\Omega)_5, (\partial\Omega)_8, \\ (\frac{\rho_l K_{rl} K}{\mu_l} \frac{\partial p_c}{\partial s} \frac{\partial s}{\partial n})|_{cl} = (D_\lambda \frac{\partial \lambda}{\partial n})|_m & \text{on } (\partial\Omega)_6, (\partial\Omega)_7, \\ \frac{\partial s}{\partial n} = 0 & \text{otherwise}. \end{array} \tag{17}$$

The Dirichlet boundary condition is proposed on the interfaces of CL and membrane for the water content equation in membrane (13):

$$\begin{array}{ll} \lambda = \lambda_{cl,m} & \text{on } (\partial\Omega)_6, (\partial\Omega)_7, \\ \frac{\partial\lambda}{\partial n} = 0 & \text{otherwise}, \end{array} \tag{18}$$

where $\lambda_{cl,m}$ is defined in Table 1.

3. Numerical simulation methods

3.1. Weak forms

To define finite element discretizations for the governing equations (1), (2), (4), (12) and (13), we shall derive their weak forms first in terms of the corresponding boundary conditions.

Let Ω be the computational domain, shown in Fig.1, and define

$$\begin{aligned} V &:= \{\vec{v} = (v_1, v_2)^\top \in [H^1(\Omega)]^2 \mid v_1|_{(\partial\Omega)_1\cup(\partial\Omega)_2} = u_1|_{inlet}, v_2|_{(\partial\Omega)_1\cup(\partial\Omega)_2} = 0\}, \\ \widetilde{V} &:= \{\vec{v} = (v_1, v_2)^\top \in [H^1(\Omega)]^2 \mid v_1|_{(\partial\Omega)_1\cup(\partial\Omega)_2} = 0, v_2|_{(\partial\Omega)_1\cup(\partial\Omega)_2} = 0\}, \\ P &:= L^2(\Omega), \\ Q &:= \{w \in H^1(\Omega) \mid w|_{(\partial\Omega)_1\cup(\partial\Omega)_2} = C_{in}\}, \quad \widetilde{Q} := \{w \in H^1(\Omega) \mid w|_{(\partial\Omega)_1\cup(\partial\Omega)_2} = 0\}, \\ X &:= \{l \in H^1(\Omega) \mid l|_{(\partial\Omega)_5\cup(\partial\Omega)_8} = s_{cl,m}\}, \quad \widetilde{X} := \{l \in H^1(\Omega) \mid l|_{(\partial\Omega)_5\cup(\partial\Omega)_8} = 0\}, \\ Z &:= \{z \in H^1(\Omega) \mid z|_{(\partial\Omega)_6\cup(\partial\Omega)_7} = \lambda_{cl,m}\}, \quad \widetilde{Z} := \{z \in H^1(\Omega) \mid z|_{(\partial\Omega)_6\cup(\partial\Omega)_7} = 0\}. \end{aligned}$$

Then for any $(\vec{v}, q, w, l, z) \in \widetilde{V} \times P \times \widetilde{Q} \times \widetilde{X} \times \widetilde{Z}$, find $(\vec{u}_g, p_g, C_w, s, \lambda) \in V \times P \times Q \times X \times Z$, such that

$$\begin{cases} (\mu_g \nabla\vec{u}_g, \nabla\vec{v}) + (\frac{\rho_g}{\varepsilon^2(1-s)^2}\nabla\cdot(\vec{u}_g\vec{u}_g), \vec{v}) - (p_g, \nabla\cdot\vec{v}) + (\frac{\mu_g}{(1-s)^3K}\vec{u}_g, \vec{v}) = 0 \\ (\nabla\cdot\vec{u}_g, q) = 0 \\ (\nabla\cdot(\vec{u}_g C_w), w) + (D_w^{eff}\nabla C_w, \nabla w) - \int_{(\partial\Omega)_6\cup(\partial\Omega)_7} D_w^{eff}\frac{\partial C_w}{\partial n} w d\tau = (S_w, w) \\ (\frac{\rho_l K s^3}{\mu_l}\frac{\partial p_c}{\partial s}\nabla s, \nabla l) + (\frac{\rho_l\mu_g s^2\vec{u}_g}{\mu_l(1-s)^3}s, \nabla l) - \int_{(\partial\Omega)_6\cup(\partial\Omega)_7}\frac{\rho_l K s^3}{\mu_l}\frac{\partial p_c}{\partial s}\frac{\partial s}{\partial n} l d\tau = (-S_{vl}W_w, l) \\ (D_\lambda\nabla\lambda, \nabla z) = (S_\lambda, z), \end{cases} \tag{19}$$

which $(\cdot,\cdot)$ stands for the L^2 inner product in Ω.

3.2. Two-grid method

Let $\mathcal{T}_h$ be a rectangular partition of Ω with the maximum mesh size h. $S_h = V_h \times P_h \times Q_h \times X_h \times Z_h \subset V \times P \times Q \times X \times Z$ and $\widetilde{S}_h = \widetilde{V}_h \times P_h \times \widetilde{Q}_h \times \widetilde{X}_h \times \widetilde{Z}_h \subset \widetilde{V} \times P \times \widetilde{Q} \times \widetilde{X} \times \widetilde{Z}$ be the piecewise bilinear finite element spaces.

In comparison to the relatively small diffusion coefficients, the convection coefficients arising in momentum and concentration equations are dominant due to large flow in the gas channel, which inevitably induces numerical instability and oscillating solution. It is crucial to design a robust numerical scheme to efficiently solve convection-dominated diffusion equations. To combine the advantages of both upwind finite volume scheme and finite element method, and conquer the dominant convection effect in the framework of finite element approach, we employ a combined finite element-upwind finite volume method [28, 29, 14] for the PEMFC model in this section, where a finite volume based finite-difference upwind scheme is adopted to specifically deal with dominant convection term only, meanwhile, all the other terms are still discretized by finite element method.

Without loss of generality, let us choose the convection term $\frac{\rho_g}{\varepsilon^2(1-s_h^k)^2}(\nabla\cdot((\vec{u}_g)_h^k(\vec{u}_g)_h^{k+1}), \vec{v}_h)$ in equation (2) to demonstrate how the combined finite element-upwind finite method works for the PEMFC model. Based on the dual mesh of $\mathcal{T}_h$, shown in Fig. 2 for example, we derive the following finite volume discretization:

$$\begin{aligned} & n((\vec{u}_g)_h^k, (\vec{u}_g)_h^{k+1}, s_h^k, \vec{v}_h) = \frac{\rho_g}{\varepsilon^2(1-s_h^k)^2}(\nabla\cdot((\vec{u}_g)_h^k(\vec{u}_g)_h^{k+1}), \vec{v}_h) \\ & \approx \sum_{i=1}^{N} v_i \sum_{P_j\in\partial\Lambda_i} \frac{\rho_g}{\varepsilon^2(1-s_h^k)^2}\int_{\Gamma_{ij}}((\vec{u}_g)_h^k\cdot\vec{n})ds(r_{ij}(\vec{u}_g)_{h,i}^{k+1} + (1-r_{ij})(\vec{u}_g)_{h,j}^{k+1}) \end{aligned} \tag{20}$$

where $r_{ij}$is the upwind parameter, automatically determined by the following formula:

$$r_{ij} = \begin{cases} 1 & \text{if } F_{ij} > 0, \\ 0 & \text{if } F_{ij} < 0, \\ 0.5 & \text{if } F_{ij} = 0, \end{cases} \tag{21}$$

where $F_{ij} = \int_{\Gamma_{ij}} ((\vec{u}_g)_h^k \cdot \vec{n}) ds$ is called numerical flux, and the reader with interest can refer to [12] for more details.

Similarly, the convection term $(\nabla \cdot ((\vec{u}_g)_h^{k+1}(C_w)_h^{k+1}), w_h)$ in equation (4) can be discretized as follows:

$$n((\vec{u}_g)_h^{k+1}, (C_w)_h^{k+1}, w_h) = (\nabla \cdot ((\vec{u}_g)_h^{k+1}(C_w)_h^{k+1}), w_h) \approx \sum_{i=1}^{N} w_i \sum_{P_j \in \partial\Lambda_i} \int_{\Gamma_{ij}} ((\vec{u}_g)_h^{k+1} \cdot \vec{n}) ds (r_{ij}(C_w)_{h,i}^{k+1} + (1 - r_{ij})(C_w)_{h,j}^{k+1})$$

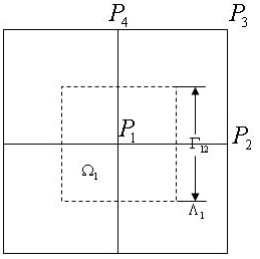

Figure 2: Control volume Ω_1 in dual mesh encompassed by broken lines in patch Λ_1.

3.2.1. The conventional method

The conventional finite element method are carried out by discretizing the nonlinear system as follows. Provided that $((\vec{u}_g)_h^k, (p_g)_h^k, (C_w)_h^k, s_h^k, \lambda_h^k)$ are given, for any $(\vec{v}_h, q_h, w_h, l_h, z_h) \in \widetilde{S}_h$, find $((\vec{u}_g)_h^{k+1}, (p_g)_h^{k+1}, (C_w)_h^{k+1}, s_h^{k+1}, \lambda_h^{k+1}) \in S_h$, the following discretizations of governing equations hold $(k = 0, 1, 2...)$

$$\begin{cases} (\mu_g \nabla(\vec{u}_g)_h^{k+1}, \nabla\vec{v}_h) + n((\vec{u}_g)_h^k, (\vec{u}_g)_h^{k+1}, s_h^k, \vec{v}_h) - ((p_g)_h^{k+1}, \nabla \cdot \vec{v}_h) + (\frac{\mu_g}{(1-s_h^k)^3 K}(\vec{u}_g)_h^{k+1}, \vec{v}_h) + \delta(h^2)(\nabla(p_g)_h^{k+1}, \nabla q_h) = 0 \\ (\nabla \cdot (\vec{u}_g)_h^{k+1}, q_h) = 0 \\ n((\vec{u}_g)_h^{k+1}, (C_w)_h^{k+1}, w_h) + ((D_w^{eff})_h^k \nabla(C_w)_h^{k+1}, \nabla w_h) - \int_{(\partial\Omega)_6 \cup \partial\Omega)_7} (D_\lambda \frac{\partial\lambda}{\partial n})_h^k w_h d\tau = ((S_w)_h^k, w_h) \\ ((\frac{\rho_l K s^3}{\mu_l} \frac{\partial p_c}{\partial s})_h^k \nabla s_h^{k+1}, \nabla l_h) + ((\frac{\rho_l \mu_g s^2 \vec{u}_g}{\mu_l (1-s)^3})_h^k s_h^{k+1}, \nabla l_h) - \int_{(\partial\Omega)_6 \cup \partial\Omega)_7} (D_\lambda \frac{\partial\lambda}{\partial n})_h^k l_h d\tau = ((-S_{vl} W_w)_h^k, l_h) \\ ((D_\lambda)_h^k \nabla \lambda_h^{k+1}, \nabla z_h) = ((S_\lambda)_h, z_h), \end{cases} \tag{22}$$

where a pressure-stabilizing term $\delta(h^2)(\nabla(p_g)_h, \nabla q_h)$ is added to momentum equation in order to ensure that the adopted Q1Q1 element is stable.

3.2.2. The two-grid algorithm

To compute the approximation solution of the nonlinear PDEs with less computational cost and the same optimal order of convergence, the two-grid method plays a crucial role in the following numerical simulation of fuel cell.

Step 1. Given $((\vec{u}_g)_H^0, (p_g)_H^0, (C_w)_H^0, s_H^0, \lambda_H^0)$, solve the nonlinear problem on coarse mesh $\mathcal{T}_H$, i.e. iteratively solve (22) for $((\vec{u}_g)_H^{k+1}, (p_g)_H^{k+1}, (C_w)_H^{k+1}, s_H^{k+1}, \lambda_H^{k+1}) \in S_H$ until $(k = 0, 1, 2...)$

$$\|(\vec{u}_g)_H^{k+1} - (\vec{u}_g)_H^k\|_0 + \|(p_g)_H^{k+1} - (p_g)_H^k\|_0 + \|(C_w)_H^{k+1} - (C_w)_H^k\|_0 + \|s_H^{k+1} - s_H^k\|_0 + \|\lambda_H^{k+1} - \lambda_H^k\|_0 < \text{tolerance}. \tag{23}$$

Step 2. Solve the following linear problem (24) on fine mesh $\mathcal{T}_h$ to obtain the approximate solutions $((\vec{u}_g)_h, (p_g)_h, (C_w)_h, s_h, \lambda_h) \in S_h$.

$$\begin{cases} (\mu_g \nabla(\vec{u}_g)_h, \nabla\vec{v}_h) + n((\vec{u}_g)_H, (\vec{u}_g)_h, s_H, \vec{v}_h) - ((p_g)_h, \nabla\cdot\vec{v}_h) + (\frac{\mu_g}{(1-s_H)^3 K}(\vec{u}_g)_h, \vec{v}_h) + \delta(h^2)(\nabla(p_g)_h, \nabla q_h) = 0 \\ (\nabla\cdot(\vec{u}_g)_h, q_h) = 0 \\ n((\vec{u}_g)_h, (C_w)_h, w_h) + ((D_w^{eff})_H \nabla(C_w)_h, \nabla w_h) - \int_{(\partial\Omega)_6 \cup \partial\Omega)_7} (D_\lambda \frac{\partial\lambda}{\partial n})_H w_h d\tau = ((S_w)_H, w_h) \\ ((\frac{\rho_l K s^3}{\mu_l}\frac{\partial p_c}{\partial s})_H \nabla s_h, \nabla l_h) + ((\frac{\rho_l \mu_g s^2 \vec{u}_g}{\mu_l (1-s)^3})_H s_h, \nabla l_h) - \int_{(\partial\Omega)_6 \cup \partial\Omega)_7} (D_\lambda \frac{\partial\lambda}{\partial n})_H l_h d\tau = ((-S_{vl} W_w)_H, l_h) \\ ((D_\lambda)_H \nabla\lambda_h, \nabla z_h) = (-S_\lambda, z_h), \end{cases} \tag{24}$$

Since the two-grid algorithm only solve the nonlinear equations on the coarse grid and solve the linear equations on the fine grid, the computational cost of nonlinear iteration is greatly reduced, which validated by the following numerical experiments.

4. Numerical results

In this section, we carry out the following numerical experiments which indicate that our methods are effective and fast to deal with PEMFC simulation. It is well known that the flow profile is parabolic under steady flow conditions once laminar flow is fully developed in long and straight channel. Based on this fact, in the following numerical experiments, we assign the Dirichlet boundary condition of velocity at the inlet as follows

$$u_1|_{inlet} = \begin{cases} u_{in,c}\sin(y\pi/\delta_{CH}) & \text{at cathode inlet } (\partial\Omega)_2 \\ u_{in,a}\sin((y-\delta_{ca})\pi/\delta_{CH}) & \text{at anode inlet } (\partial\Omega)_1 \end{cases} \quad 0 \le y \le \delta_{CH}, \tag{25}$$

where $\delta_{ca} = \delta_{CH} + \delta_{GDL} + \delta_{CL} + \delta_{mem}$.

Since the liquid water has a slight motion exists in channel width direction and increases along channel direction [5], we assume the liquid water along channel has a linear change, from the minimum value to the maximum value.

$$s_{CH,GDL} = 0.1(l_{cell} - x)/l_{cell} + 0.2x/l_{cell}. \tag{26}$$

In order to verify the correctness and efficiency of our two-grid numerical solutions, we compute the relative error of mass balance and simulation time with the boundary condition of $u_{in,a} = 5\ m/s, u_{in,c} = 3\ m/s, C_{in,a} = 10\ mol/m^3, C_{in,c} = 12\ mol/m^3$ compared with the conventional finite element method in our following simulations. And the tolerance of our stopping criteria (23) for iteration is 10^{-8}. An example of a coarse and a fine mesh size for the two-grid method is present in Fig.3. And Table 4 shows that our two-grid method can cut down the compute time dramatically with non-losing accuracy.

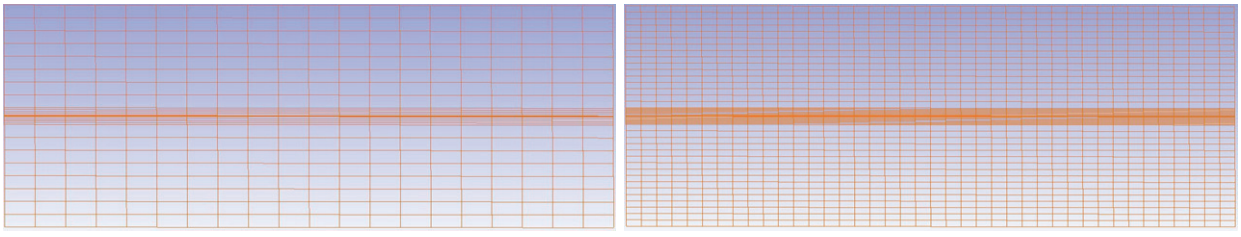

Figure 3: An example of coarse grid (left) and fine grid (right) for two-grid method

Fig. 4 show the velocity field in anode and cathode of fuel cell produced by the two-grid method and the conventional method, which shows the same numerical results completely. As expected, there is a large difference in the velocity scale between the porous media and the open channel. The velocity in porous GDL is at least two orders of magnitude smaller than that in the open gas channel, indicating that gas diffusion is the dominant transport mechanism in porous GDL. Porous CL has a smaller velocity than GDL due to the inferior diffusion ability.

Fig. 5 and Fig. 6 show the contours of the vapor water concentration and liquid water saturation in cathode respectively. Due to water production by fuel cell, a small amount of liquid water emerges downstream, i.e., liquid

Table 4: Mass balance error and compute time

Fine mesh size	Conventional method		Two-grid method		
	Mass balance error	Time	Coarse mesh size	Mass balance error	Time
20×36	2.166e-003	74s	10×18	2.168e-003	114s
40×72	1.680e-003	115s	20×36	1.680e-003	128s
80×144	1.110e-003	639s	40×72	1.110e-003	294s
160×288	4.111e-004	3351s	80×144	4.004e-004	1750s

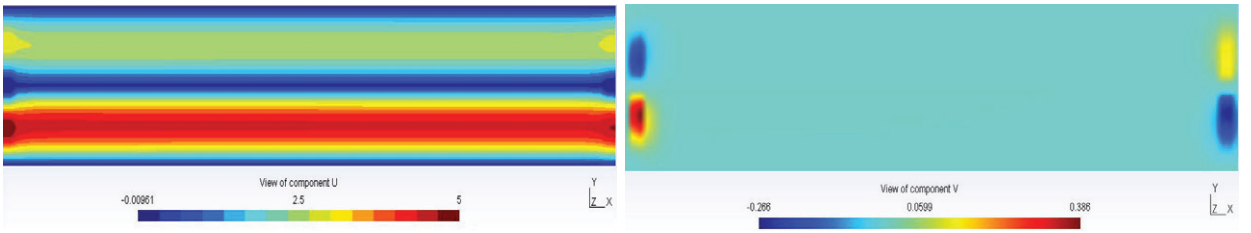

Figure 4: Horizontal and vertical gas velocities in PEMFC produced by two-grid method

water saturation $s > 0$ there, and the flow in the diffusion layer shifts to gas water multiphase flow. Once liquid water is being created by condensation, it is dragged into the GDL by the gas phase, the liquid water can only exit the GDL through the build-up of a capillary pressure gradient to overcome the viscous drag. So the liquid saturation increased inside the GDL.

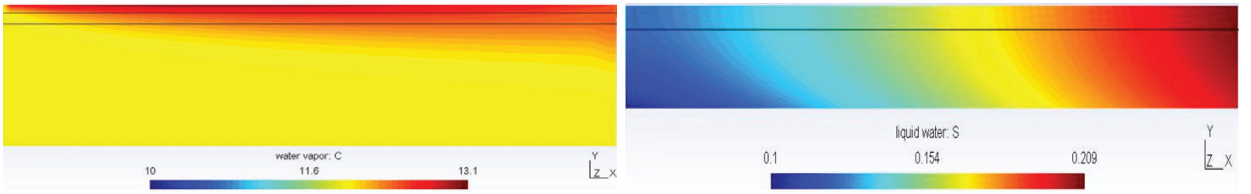

Figure 5: Vapor water concentration in cathode CL, GDL and GC

Figure 6: Liquid water saturation in cathode CL and GDL

Fig. 7 displays the water content in the membrane, which clearly shows that the water content increases from the inlet to the outlet region in the along-channel direction, presenting a complete picture of the water content variation inside the membrane.

Figure 7: Water content in membrane

5. Conclusions

In this paper, based on the combined finite element-upwind finite volume methods and the two-grid method, a new discretization scheme is designed and implemented for a simplified two-phase 2D mixed-domain fuel cell model. Numerical experiments demonstrate that our methods are able to solve the governing equations with less compute

time, and obtain a relatively accurate numerical solution with low mass balance error. The two-grid method will greatly decrease the computational amount, and improve the computing speed and accuracy for 3D PEMFC model, therefore the two-grid method for 3D two-phase mixed-domain complete model will be studied in our future work.

Acknowledgments

The supports from NSFC (Grants No.11101311) and "Applied Mathematics Chair Fund of China-German College" (0900101021) are fully acknowledged. And Pengtao Sun is supported in part by NSF Grant DMS-0913757.

References

[1] Z. Wang, C. Wang, K. Chen, Two-phase flow and transport in the air cathode of proton exchange membrane fuel cells, Journal of Power Sources 94 (2001) 40–50.
[2] C. Wang, Fundamental models for fuel cell engineering, Journal of the Electrochemical Society 104 (2004) 4727–4766.
[3] H. Meng, C. Wang, Large-scale simulation of polymer electrolyte fuel cells by parallel computing, Chemical Engineering Science 59 (2004) 3331–3343.
[4] U. Pasaogullari, C. Wang, Two-phase modeling and flooding prediction of polymer electrolyte fuel cells, Journal of Electrochemical Soceity 152 (2005) A380–A390.
[5] Y. Wang, S. Basu, C. Wang, Modeling two-phase flow in PEM fuel cell channels, Journal of power source 179 (2008) 603–617.
[6] B. Sivertsena, N. Djilalib, Three-dimensional computational analysis of transport phenomena in a pem fuel cell, Journal of Power Sources 106 (2002) 284–294.
[7] G. He, P. Ming, Z. Zhao, A two-fluid model for two-pahse flow in pemfcs, Journal of Power Sources 163 (2007) 864–873.
[8] T. Berning, Three-dimensional computational analysis of transport phenomena in a PEM fuel cell, Doctor of philosophy, University of Victoria (2002).
[9] W. Tao, C. Min, X. Liu, Y. He, B. Yin, W. Jiang, Parameter sensitivity examination and discussion of pem fuel cell simulation model validation part I. current status of modeling research and model development, Journal of Power Sources 160 (2006) 359–373.
[10] C. hua Min, A novel three-dimensional, two-phase and non-isothermal numerical model for proton exchange membrane fuel cell, Journal of Power Sources 195 (2010) 1880–1887.
[11] H. Meng, A two-phase non-isothermal mixed-domain pem fuel cell model and its application to two-dimensional simulations, Journal of Power Sources 168 (2007) 218–228.
[12] P. Sun, G. Xue, C. Wang, J. Xu, A domain decomposition method for two-phase transport model in the cathode of a polymer electrolyte fuel cell, Journal of Computational Physics 228 (2009) 6016–6036.
[13] P. Sun, G. Xue, C. Wang, J. Xu, Fast numerical simulation of two-phase transport model in the cathode of a polymer electrolyte fuel cell, Communications in Computational Physics 6 (2009) 49–71.
[14] P. Sun, G. Xue, C. Wang, J. Xu, A combined finite element-upwind finite volume-newton's method for liquid feed direct methanol fuel cell simulations, in: Engineering, T. Conference (Eds.), Proceeding of Sixth International Fuel Cell Science, 2008.
[15] P. Sun, Modeling studies and efficient numerical methods for proton exchange membrane fuel cell, Computer Methods in Applied Mechanics and Engineering 200 (2011) 3324–3340.
[16] P. Sun, S. Zhou, Q. Hu, G. Liang, Numerical study of a 3D two-phase pem fuel cell odel via a novel automated finite element/finite volume program generator, Communications in Computational Physics 11 (2012) 65–98.
[17] M. He, Z. Huang, C. Wang, P. Sun, An overlapping domain decomposition method for a polymer exchange membrane fuel cell model, Procedia Computer Science 4 (2011) 1343–1352.
[18] J. Xu, A new class of iterative methods for nonselfadjoint or indefinite problems, SIAM journal on numerical analysis 29 (1992) 303–319.
[19] J. Xu, Two-grid discretization techniques for linear and nonlinear pdes, SIAM journal on numerical analysis 33 (1996) 1759–1777.
[20] O. Axelsson, W. Layton, A two-level discretization of nonlinear boundary value problems, SIAM journal on numerical analysis 33 (1996) 2359–2374.
[21] C. Dawson, C. Woodward, M. Wheeler, A two-grid finite difference scheme for nonlinear parabolic equations, SIAM journal on numerical analysis 35 (1998) 435–452.
[22] R. Bank, M. Holst, A new paradigm for parallel adaptive meshing algorithms, SIAM journal on Scientific Computing 22 (2000) 1411–1443.
[23] Y. He, J. Xu, A. Zhou, Local and parallel finite element algorithms for the stokes problem, Numerische Mathematik 109 (2008) 415–434.
[24] Y. He, J. Xu, A. Zhou, local and parallel finite element algorithms for the navier-stokes problem, Journal of Computational Mathematics 24 (2006) 227–238.
[25] H. Meng, A three-dimensional pem fuel cell model with consistent treatment of water transport in mea, Journal of Power Sources 162 (2006) 426–435.
[26] S. Um, C. Wang, Computational study of water transport in proton exchange membrane fuel cells, Journal of Power Sources 156 (2006) 211–223.
[27] J. H. Nam, M. Kaviany, Effective diffusivity and water-saturation distribution in single-and two-layer pemfc diffusion medium, International Journal of Heat and Mass Transfer 46 (2003) 4595–4611.
[28] D. Kroner, M. Rokyta, Convergence of upwind finite volume schemes for scalar conservation laws in two dimensions, SIAM Journal on Numerical Analysis 31 (1994) 324–343.
[29] M. Feistauer, J. Felcman, On the convergence of a combined finite volume-finite element for nonlinear convectioncdiffusion problems, Numerical Methods for Partial Differential Equations 13 (1997) 163–190.